Model Based Image Reconstruction with Physics Based Priors

Muhammad Usman Sadiq[†], Jeff. P. Simmons[*], Charles A. Bouman[†]
[†]School of Electrical and Computer Engineering, Purdue University, West Lafayette, IN, 47907, USA
[*]Air Force Research Laboratory, Wright-Patterson AFB, OH 45433

***Abstract*—Computed tomography is increasingly enabling scientists to study physical processes of materials at micron scales. The MBIR framework provides a powerful method for CT reconstruction by incorporating both a measurement model and prior model. Classically, the choice of prior has been limited to models enforcing local similarity in the image data. In some material science problems, however, much more may be known about the underlying physical process being imaged. Moreover, recent work in Plug-And-Play decoupling of the MBIR problem has enabled researchers to look beyond classical prior models, and innovations in methods of data acquisition such as interlaced view sampling have also shown promise for imaging of dynamic physical processes.**

In this paper, we propose an MBIR framework with a physics based prior model - namely the Cahn-Hilliard equation. The Cahn-Hilliard equation can be used to describe the spatio-temporal evolution of binary alloys. After formulating the MBIR cost with Cahn-Hilliard prior, we use Plug-And-Play algorithm with ICD optimization to minimize this cost. We apply this method to simulated data using the interlaced-view sampling method of data acquisition. Results show superior reconstruction quality compared to the Filtered Back Projection. Though we use Cahn-Hilliard equation as one instance, the method can be easily extended to use any other physics-based prior model for a different set of applications.

I. Introduction

Computed tomography is witnessing increasing use for imaging of materials at micron scales, and the model based image reconstruction(MBIR) framework has proved to be a powerful tool for solving inverse problems in computed tomography [1]–[3]. The MBIR framework has been successfully applied to helical CT [4], BF electron tomography [5] and synchrotron X-ray CT [6], producing better quality reconstructions from fewer views and reducing noise and artifacts.

MBIR algorithms incorporate a measurement model [7], statistical noise model [8], and a prior model [9]. However, the classical choice of priors to be used in the MBIR framework has been under discussion recently [10]. Conventionally, MBIR prior models have been based on local neighborhood operations such as Markov-Random-Fields [4]. which penalize the dissimilarity between neighboring voxels using a neighborhood based penalty function.

In contrast, some other methods which exploit non-local patterns have also been employed for solving inverse problems. These methods include bilateral filtering [11], non-local means [10], [12], [13], BM3D denoising [14], and k-SVD [15].

However, in some applications, the object being imaged is known to obey certain well-defined physical model equations. For example, phase-field equations model the evolution in time and space of the phases of a material, and are typically used to model separation of the liquid and solid phases during the solidification of a metal. A widely used phase-field model is known as the Cahn-Hilliard equation, which consists of a partial differential equation in space and time that models the evolution of the binary phases [16]. Interestingly, some earlier work has connected phase-field models with image processing in applications such such as segmentation, denoising [17], [18] and image in-painting [19].

In this paper, we propose an MBIR framework for inverse problems with a physics-based prior, based on a phase-field model known as the Cahn-Hilliard equation. We used the physics-based model of the Cahn-Hilliard equations to create a prior distribution that constrains the form of the reconstruction in space and time. This is unique since prior models are typically ad-hoc distributions or empirically trained from an ensemble of example data. Since this is a strong prior than conventionally used ones, we demonstrate that this prior can reconstruct the phase separation process using a limited set of interlaced view samples. Thus, the method can be used to perform a 4D reconstruction using a 3D helical manifold. Though our method can not be applied directly to medical imaging, there may be other appropriate physical models for specific applications in medical imaging that can be used as priors.

One challenge in applying such a physics-based prior for MBIR is the difficulty in optimizing the resulting MBIR cost function [10]. Our approach is to use the Plug-And-Play algorithm [20] to decoupling of the forward and prior models, thereby easing inclusion of physics based prior. We apply our algorithm to simulated data using interlaced view samples and demonstrate better reconstruction quality than the Filtered Back Projection reconstruction.

II. The Cahn-Hilliard Equations

For a binary fluid with concentration $u(r_x, r_y, t)$, the Cahn-Hilliard equation is given by

$$\frac{\partial u}{\partial t} = M\nabla^2\left(-\epsilon^2\nabla^2 u + \frac{df}{du}\right) \tag{1}$$

where M is a diffusion coefficient ($length^2/time$), ϵ gives the coefficient of gradient energy ($length^2$) and $f(u)$ is the energy function [16]. Using a double-well energy function described in literature [21], we have $f(u) = u^2(u-1)^2$ such that $f'(u) = 4u^3 - 6u^2 + 2u$ for our purposes. Intuitively, $0 \leq u(r_x, r_y, t) \leq 1$ represents the local concentration of the binary phase with, for example, $u = 0$ representing liquid phase and $u = 1$ representing solid phase. Equation (1) can

be simplified to the form

$$\frac{\partial u}{\partial t} = -\tilde{a}\nabla^4 u + \tilde{b}\nabla^2 f'(u) \tag{2}$$

where $\tilde{a} = M\epsilon^2$, $\tilde{b} = M$.

We formulate the model in 3D with two spatial dimensions and time. So the discretized version of u is given by

$$u_{n,i,j} = u(i\Delta_x, j\Delta_x, n\Delta_s) \ ,$$

where Δ_x and Δ_t are the discretization steps in space and time, respectively; and the discrete indices range over $n \in \{1, \cdots, N_t\}$ and $i, j \in \{1, \cdots, N_x\}$. In addition, we use u_n to denote each $N_x \times N_x$ image at time n.

In order to discretize the Cahn-Hilliard equation, we first define the operator

$$[Du_n]_{i,j} = u_{n,i+1,j} + u_{n,i-1,j} + u_{n,i,j-1} + u_{n,i,j+1} - 4u_{n,i,j} \ .$$

Then the discretized Laplacian operator is given by

$$\nabla^2 u|_{(i\Delta_x, j\Delta_x, n\Delta_s)} \simeq \frac{[D(u_n)]_{i,j}}{(\Delta_x)^2} \ .$$

Using this notation, equation (1) becomes

$$u_{n+1} - u_n = -aD(Du_n) + bD(4u_n^3 - 6u_n^2 + 2u_{n+1}) \tag{3}$$

where $a = \dfrac{\tilde{a}}{\Delta_x^4}\Delta_s$, $b = \dfrac{\tilde{b}}{\Delta_x^2}\Delta_s$.

From this, we define the function

$$\begin{aligned}[H(u,\theta)]_n =& u_{n+1} - u_n + aD(D(u_n)) \\ & - bD(4u_n^3 - 6u_n^2 + 2u_{n+1})\end{aligned} \tag{4}$$

where $\theta = [a, b]^t$ is a parameter vector. The Cahn-Hilliard equations can then be represented as

$$H(u, \theta) = 0 \ .$$

III. MBIR with the Cahn-Hilliard Prior

The goal of computed tomography is to reconstruct the attenuation coefficients from the acquired synchrotron data. We use MBIR framework to perform this reconstruction. The generic form of maximum a posteriori (MAP) reconstruction is given by

$$\hat{u} = \underset{u}{\operatorname{argmin}} \left(-\log p(y|u, \phi) - \log p(u) \right) \ . \tag{5}$$

where y represents the vector of noisy projection measurements obtained from the physical system and u encodes the solution to the phase-field as a column vector. Then employing a widely used X-ray transmission model [22], the first term in (5) can be approximated as

$$-logp(y|u) \approx ||y - Au||_\Lambda^2 + h(y) \ .$$

where A is the forward projection matrix, and Λ is a diagonal matrix of detector photon counts for each projection.

Using this approximation and the parameterized Cahn-Hilliard function of (4), the MAP estimate with the Cahn-Hilliard prior is given by

$$\hat{u} = \underset{u}{\operatorname{argmin}} \left(\frac{1}{2}||y - Au||_\Lambda^2 + \frac{1}{2\sigma_H^2} \frac{||H(u,\theta)||^2}{N_t N_x^2} \right) \tag{6}$$

Notice that the prior term in equation (6) implies that the MAP estimate should approximately solve the Cahn-Hilliard equations. The accuracy of that approximation can be controlled through the selection of the parameter σ_H. As σ_H approaches 0, the Cahn-Hilliard equations are exactly solved. But as the value of Cahn-Hilliard regularization increases, then some approximation in the solution is allowed.

IV. Plug-And-Play with Cahn-Hilliard De-noising

In order to solve the reconstruction problem (6), we make use of the variable-splitting approach described in Plug-and-Play algorithm for Model Based Reconstruction [20]. Plug-And-Play formulation works by splitting the state variable in order to decouple the forward model and prior terms of MBIR problem (5), and applying the method of Alternating Directions Method of Minimization (ADMM) on the subsequent problem. This allows the MBIR reconstruction problem to be split into two decoupled problems, one for the forward model and one for the prior term.

Algorithm 1 shows the procedure for the Plug-and-Play algorithm. Notice that step 5 requires solving the tomographic inverse problem with simple quadratic regularization. Step 7 is denoising step that requires minimization of the following function.

$$g(u; z, \theta, \sigma_H, \sigma) = \frac{1}{2\sigma^2}(||z - u||_2^2) + \frac{1}{2\sigma_H^2} \frac{||H(u,\theta)||^2}{N_t N_x^2} \tag{7}$$

We minimize equation (7) as a function of u using iterative coordinate descent (ICD) optimization. For each ICD iteration, we update every voxel in $u_{n,i,j}$ by setting $[\nabla f(u)]_{n,i,j} = 0$ and solving for $u_{n,i,j}$. Since the de-noising cost (7) is not convex in $u_{n,i,j}$, if we get multiple solutions for $u_{n,i,j}$, we choose the one that minimizes the cost (7).

Algorithm 1 Plug-And-Play with Cahn-Hilliard De-noising

1: **procedure** PnPwithCH
2: Initialize $\hat{u} \leftarrow FBP(y), \eta \leftarrow 0, \hat{v} \leftarrow \hat{u}$
3: **repeat**
4: $\tilde{u} \leftarrow \hat{v} - \eta$
5: $\hat{u} \leftarrow \underset{u}{\operatorname{argmin}} \frac{1}{2}(||y - Au||_\Lambda^2) + \frac{1}{2\gamma^2}||u - \tilde{u}||_2^2$
6: $\tilde{v} \leftarrow \hat{u} + \eta$
7: **procedure** DenoiseWithCHPrior
8:

$$\hat{v} \leftarrow \underset{v}{\operatorname{argmin}} \ g(v; \tilde{v}, \theta, \sigma_H, \gamma) \tag{8}$$

9: **end procedure**
10: $\eta \leftarrow \eta + (\hat{u} - \hat{v})$
11: **until** stopping criterion is met
12: **end procedure**

V. Experimental Results

In order to demonstrate our method's performance, we apply the PnPwithCH algorithm to image the phase separation process in a phantom alloy. We use a numerically stable discretization of [21] that allows us to solve the Cahn-Hilliard equation for long times. We choose the Cahn-Hilliard parameters such that the different stages of phase separation process take place over $N_t = 64$ time instants of simulation. Instead of the conventional progressive set of views, some recent work has proposed interlaced sets of views spread over multiple half-rotations for better quality of reconstruction using limited set of view angles [6]. For a total of N_θ angles

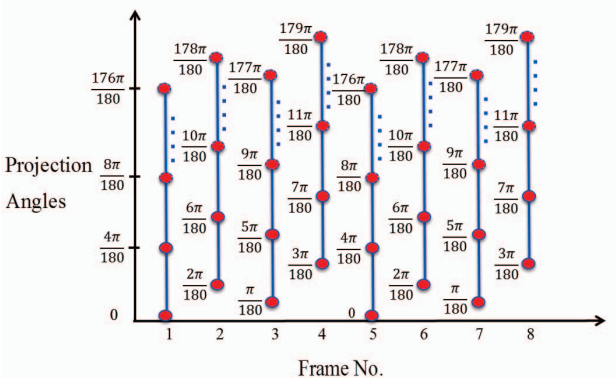

Fig. 1: Illustration of interlaced views we get with $K = 4, N_\theta = 180$

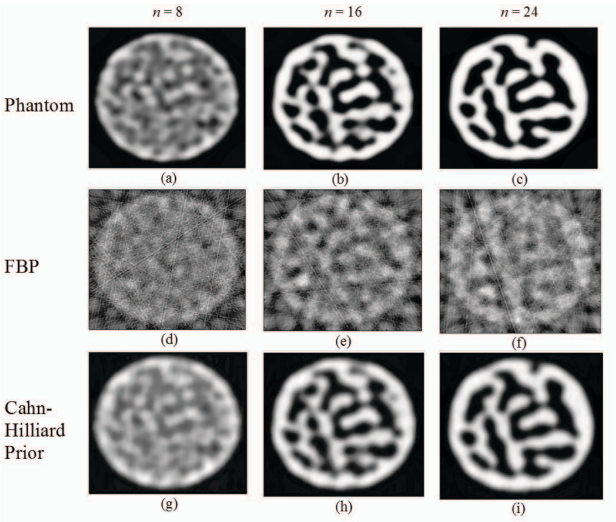

Fig. 2: Reconstruction with progressive interlaced view sampling using FBP and Cahn-Hilliard prior at different times. With $N_\theta = 64, K = 8, r = 1$, the view angles used for each reconstruction $= \frac{N_\theta}{K} r = 8$. The first row (a-c) shows the phantom. Reconstruction using FBP is shown in second row (d-f) and using MBIR with Cahn-Hilliard prior in third row (g-i)

with angular range limited to π radians, the interlaced view angles as a function of frame index n are

$$\theta_n = \left[\left(n \bmod \frac{N_\theta}{K} \right) K + \beta_r \left(\left\lfloor \frac{nK}{N_\theta} \right\rfloor \bmod K \right) \right] \frac{\pi}{N_\theta}$$

with K being the number of interlaced views, and $d = \beta_r(c)$ is the bit-reverse function which takes the binary representation of c and reverses it to produce d. This bit-reverse method has been used in literature of ordered subset methods to group projection views [23] With $N_\theta = 180, K = 4$, we illustrate the view angles we get using the interlaced view sampling in Fig 1

In Fig 2, we attempt to model the phase separation as it happens in fluid mixtures. We start with independent and identically distributed (IID) random initial conditions and

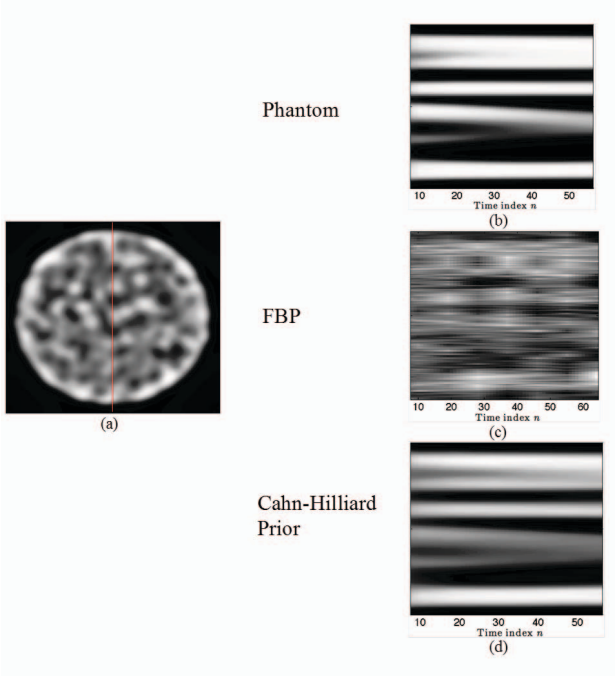

Fig. 3: Reconstruction with progressive interlaced view sampling using FBP and Cahn-Hilliard prior. (b-d) show the time evolution of a v-axis slice of the phantom(along the red line in (a))

show the different stages of phase coarsening, as modeled by Cahn-Hilliard equations in (a-c) of Fig 2. We use progressive interlaced view sampling to reconstruct this phantom data using PNPWITHCH algorithm and compare it with Filtered Back Projection. We acquire $N_\theta = 64$ distinct views over every $K = 8$ time instants, and reconstruct at a rate of $r = 1$ time sample per frame, such that we obtain $\frac{N_\theta}{K} r = 8$ views per reconstruction. We reconstruct the phantom for $N_t = 64$ time instants. In Fig. 3, we show the time evolution of a v-axis slice and its reconstruction using FBP and Cahn-Hilliard prior.

As we use only $\frac{N_\theta}{K} r = 8$ views per reconstruction to image a dynamic physical process, the FBP reconstruction exhibits bad quality as well as artifacts due to small set of views obtained. However, as we only require the initial conditions and Cahn-Hilliard parameters to completely define a Cahn-Hilliard solution, this strong prior allows us to reconstruct the whole sequence using only $\frac{N_\theta}{K} r = 8$ views per reconstruction, such that the different stages of phase separation are accurately reproduced.

The PNPWITHCH algorithm takes 10 iterations to converge. In practice, the speed of convergence of PNPWITHCH depends upon the number of views used for each reconstruction and the regularization coefficient σ_H.

Although our MBIR framework with Cahn-Hilliard prior produces almost perfect reconstruction of the phantom data, the additional problem of estimating the Cahn-Hilliard parameters may also be of interest in some applications. Therefore, we also present a first attempt to estimate θ from the reconstructed object $\hat{u}$ using $\hat{\theta} \leftarrow \underset{\theta}{\operatorname{argmin}} \frac{1}{2\sigma_H^2} ||H(\hat{u}, \theta, \Delta_s)||_2^2$. We

Simulated θ		Noise std. deviation	Estimated θ	
a	b		a	b
8	1	0.0001%	7.961	0.995
		0.001%	5.020	0.617
		0.002%	2.524	0.296
		0.003%	1.390	0.150
		0.004%	0.853	0.081
		0.005%	0.563	0.044
		0.006%	0.398	0.022
		0.007%	0.293	0.009
		0.008%	0.222	0.000
		0.009%	0.173	-0.007

Fig. 4: Illustration of sensitivity of θ estimates to noise in x

see that $\hat{\theta} = \begin{bmatrix} 0.0028 \\ 0.1591 \end{bmatrix}$ such that $\hat{\theta} \neq$ true θ, contrary to our expectation. To further investigate the reason for $\hat{\theta} \neq \theta$, we start with x such that $H(u, \theta) = 0$. Keeping the same discretization and scaling, we add White Gaussian noise to u with a range of standard deviation values and find the least-squared estimate $\hat{\theta}$ for each value of noise standard deviation. We show the $\hat{\theta}$ estimate against each value of noise standard deviation in Fig. 4.

We can see from this table that the least square estimate of θ is very sensitive to noise in u such that very small noise variance can result in deviation of $\hat{\theta}$ from true θ. This sensitivity that might be inherent from the structure of the equation can form a challenge in estimation of Cahn-Hilliard parameters in real data.

VI. Conclusions

We have provided a framework for including physics-based priors to inverse problems in imaging. This has been difficult conventionally due to tight coupling of forward and prior models in MBIR framework, resulting in difficulty in optimization. Using Plug-And-Play to decouple them, we have successfully applied MBIR with Cahn-Hilliard prior to simulated alloy data, reproducing the stages of phase separation using less data than needed with conventional methods. Therefore, our work is the first to have successfully done tomographic reconstruction using a physics based prior. Moreover, the Plug-And-Play framework we developed for the problem can be easily extended to a different prior for a different set of applications. Our results show promise for tomographic reconstruction in presence of physics-based priors in binary alloys. However, the difficulty of estimating parameters of phase-field model might pose a limitation.

References

[1] S. Venkatakrishnan, L. Drummy, M. Jackson, M. De Graef, J. Simmons, and C. Bouman, "Bayesian tomographic reconstruction for high angle annular dark field (haadf) scanning transmission electron microscopy (stem)," in *Statistical Signal Processing Workshop (SSP), 2012 IEEE*. IEEE, 2012, pp. 680–683.

[2] Z. Yu, J.-B. Thibault, C. Bouman, K. D. Sauer, J. Hsieh *et al.*, "Fast model-based x-ray CT reconstruction using spatially nonhomogeneous icd optimization," *Image Processing, IEEE Transactions on*, vol. 20, no. 1, pp. 161–175, 2011.

[3] J. Fessler *et al.*, "Penalized weighted least-squares image reconstruction for positron emission tomography," *Medical Imaging, IEEE Transactions on*, vol. 13, no. 2, pp. 290–300, 1994.

[4] J.-B. Thibault, K. D. Sauer, C. A. Bouman, and J. Hsieh, "A three-dimensional statistical approach to improved image quality for multislice helical CT," *Medical physics*, vol. 34, no. 11, pp. 4526–4544, 2007.

[5] S. V. Venkatakrishnan, L. F. Drummy, M. De Graef, J. P. Simmons, and C. A. Bouman, "Model based iterative reconstruction for bright field electron tomography," in *IS&T/SPIE Electronic Imaging*. International Society for Optics and Photonics, 2013, pp. 86 570A–86 570A.

[6] K. Mohan, S. Venkatakrishnan, J. Gibbs, E. Gulsoy, X. Xiao, M. De Graef, P. Voorhees, and C. Bouman, "TIMBIR: A method for time-space reconstruction from interlaced views," 2015.

[7] B. De Man and S. Basu, "Distance-driven projection and backprojection in three dimensions," *Physics in medicine and biology*, vol. 49, no. 11, p. 2463, 2004.

[8] J.-B. Thibault, C. A. Bouman, K. D. Sauer, and J. Hsieh, "A recursive filter for noise reduction in statistical iterative tomographic imaging," in *Electronic Imaging 2006*. International Society for Optics and Photonics, 2006, pp. 60 650X–60 650X.

[9] V. Panin, G. Zeng, and G. Gullberg, "Total variation regulated em algorithm [SPECT reconstruction]," *Nuclear Science, IEEE Transactions on*, vol. 46, no. 6, pp. 2202–2210, 1999.

[10] S. Sreehari, S. Venkatakrishnan, L. F. Drummy, J. P. Simmons, and C. A. Bouman, "Advanced prior modeling for 3d bright field electron tomography," in *IS&T/SPIE Electronic Imaging*. International Society for Optics and Photonics, 2015, pp. 940 108–940 108.

[11] A. Manduca, L. Yu, J. D. Trzasko, N. Khaylova, J. M. Kofler, C. M. McCollough, and J. G. Fletcher, "Projection space denoising with bilateral filtering and CT noise modeling for dose reduction in CT," *Medical physics*, vol. 36, no. 11, pp. 4911–4919, 2009.

[12] Y. Wu, B. Tracey, P. Natarajan, and J. P. Noonan, "James–stein type center pixel weights for non-local means image denoising," *Signal Processing Letters, IEEE*, vol. 20, no. 4, pp. 411–414, 2013.

[13] J. V. Manjón, P. Coupé, L. Martí-Bonmatí, D. L. Collins, and M. Robles, "Adaptive non-local means denoising of mr images with spatially varying noise levels," *Journal of Magnetic Resonance Imaging*, vol. 31, no. 1, pp. 192–203, 2010.

[14] K. Dabov, A. Foi, V. Katkovnik, and K. Egiazarian, "Bm3d image denoising with shape-adaptive principal component analysis," in *SPARS'09-Signal Processing with Adaptive Sparse Structured Representations*, 2009.

[15] M. Aharon, M. Elad, and A. Bruckstein, "K-svd: An algorithm for designing overcomplete dictionaries for sparse representation," *Signal Processing, IEEE Transactions on*, vol. 54, no. 11, pp. 4311–4322, 2006.

[16] J. W. Cahn and J. E. Hilliard, "Free energy of a nonuniform system. i. interfacial free energy," *The Journal of chemical physics*, vol. 28, no. 2, pp. 258–267, 1958.

[17] T. Preusser, M. Droske, C. S. Garbe, A. Telea, and M. Rumpf, "A phase field method for joint denoising, edge detection, and motion estimation in image sequence processing," *SIAM Journal on Applied Mathematics*, vol. 68, no. 3, pp. 599–618, 2007.

[18] Y. M. Jung, S. H. Kang, and J. Shen, "Multiphase image segmentation via modica-mortola phase transition," *SIAM Journal on Applied Mathematics*, vol. 67, no. 5, pp. 1213–1232, 2007.

[19] A. L. Bertozzi, S. Esedoglu, and A. Gillette, "Inpainting of binary images using the cahn-hilliard equation," *IEEE Transactions on image processing*, vol. 16, no. 1, pp. 285–291, 2007.

[20] S. Venkatakrishnan, C. Bouman, B. Wohlberg *et al.*, "Plug-and-play priors for model based reconstruction," in *Global Conference on Signal and Information Processing (GlobalSIP), 2013 IEEE*. IEEE, 2013, pp. 945–948.

[21] J.-W. Choi, H. G. Lee, D. Jeong, and J. Kim, "An unconditionally gradient stable numerical method for solving the allen–cahn equation," *Physica A: Statistical Mechanics and its Applications*, vol. 388, no. 9, pp. 1791–1803, 2009.

[22] K. Sauer and C. Bouman, "Bayesian estimation of transmission tomograms using segmentation based optimization," *Nuclear Science, IEEE Transactions on*, vol. 39, no. 4, pp. 1144–1152, 1992.

[23] D. Kim, S. Ramani, J. Fessler *et al.*, "Combining ordered subsets and momentum for accelerated x-ray CT image reconstruction," *Medical Imaging, IEEE Transactions on*, vol. 34, no. 1, pp. 167–178, 2015.